CFD analysis of the impact of air gap width on Trombe wall performance

Received: 18 June 2024 | Revised: 16 August 2024 | Accepted: 22 August 2024

DOI: 10.1002/ese3.1913

ORIGINAL ARTICLE

CFD analysis of the impact of air gap width on Trombe wall performance

Khaoula Friji[1] | **Ons Ghriss**[2] | **Abdallah Bouabidi**[3] | **Erdem Cuce**[4,5,6] | **Saad Alshahrani**[7,8]

[1]Mechanical Modelling, Energy & Materials (M2EM) Laboratory, LR24ES23, National Engineering School of Gabès, University of Gabes, Gabes, Tunisia

[2]Engineering School of Gabes (ENIG), RL Processes, Energetic, Environment, and Electric Systems, University of Gabes, Gabes, Tunisia

[3]Higher Institute of Industrial Systems of Gabes (ISSIG), University of Gabes, Gabes, Tunisia

[4]Department of Mechanical Engineering, Faculty of Engineering and Architecture, Recep Tayyip Erdogan University, Rize, Turkey

[5]Department of Mechanical Engineering, College of Engineering, Birmingham City University, Birmingham, UK

[6]University Centre for Research and Development, Chandigarh University, Mohali, India

[7]Department of Mechanical Engineering, College of Engineering, King Khalid University, Abha, Saudi Arabia

[8]Centre for Engineering and Technology Innovations, King Khalid University, Abha, Saudi Arabia

Correspondence
Erdem Cuce, Department of Mechanical Engineering, Faculty of Engineering and Architecture, Recep Tayyip Erdogan University, Zihni Derin Campus, 53100 Rize, Turkey.
Email: erdem.cuce@erdogan.edu.tr

Abstract

In recent years, there has been a lot of research and debate on how solar energy can be used instead of conventional sources of heating to power residential heating. In this study, the Trombe wall (TW) technique, based on natural convection and energy storage, was examined to predict mass flow rate, temperature field, and velocity field for the TW system under steady conditions. A numerical simulation model was investigated for further validation using k-ε turbulence and discrete ordinates (DO) radiation models. Independent grid studies were conducted to ensure that there were no changes after varying the grid numbers. The effect of the air gap was carried out to enhance TW thermal performance. CFD simulation shows good agreement with published data in the literature, and the optimum air gap was set at 0.1 m. The results pave the way for future studies to improve passive solar heating systems, which will eventually help move towards more sustainable residential heating solutions.

KEYWORDS

CFD, natural ventilation, solar radiation, Trombe wall

1 | INTRODUCTION

The use of fossil fuels for heating and electricity production has contributed significantly to climate change by releasing large volumes of carbon dioxide into the atmosphere. It is vital to move away from fossil fuels and toward clean, sustainable energy sources to address these problems.[1] The architectural and thermal planning of the widely recognised Trombe wall (TW) represents a well-established approach to conserving energy within the construction industry. TW comprises a substantial wall surface enclosed by external glazing. It functions as a passive heating and cooling system that capitalises on solar irradiation and fluctuations in ambient temperature to effectively accumulate energy and subsequently release it into the indoor environment at the most reasonable times and an appropriate rate. Other prevalent passive systems include the solar chimney, the unglased transpired solar façade, and green walls.[2]

Recent studies have explored various aspects of TWs, demonstrating their potential in reducing energy consumption. However, Abbassi et al.[3] developed a numerical model on the solar heating system wall of Trombe and validated it with a small-scale experimental study located in Tunisia. The results showed that the TW of 4 m^2 surface could cover about 50% of the energy demand of the annual heating of a Tunisian building, and the 8 m^2 surface can cover up to 77%. Moreover, they also showed that a TW area of 3 m^2 leads to a heating energy reduction of 63%.

Z. Hu et al.[4] presented a new wall of Trombe with blinds for shading and a water flow system (WBTW). Nevertheless, simulation results show that the WBTW system is more efficient than others, offering satisfactory insulation in winter and reducing the annual thermal load by 42.6% with an energy collection of 435.7 kWh, compared to 13.6% and 20.3 kWh for other systems.

Li et al.[5] combined mathematical and numerical methods to analyse the air velocity pattern. The outcomes demonstrate that the increase in the TW height or the temperature difference between the glass and the massive wall leads to the rise in the air velocity inside the TW. Although the traditional TW shows significant thermal performance, its thermal resistance is very low during the night, representing the major disadvantage of this system.

I. Hernandez-Lopez et al.[6] performed a thermal evaluation of a room containing a TW during the hottest and coldest days in two cities in Mexico. Although the glass cover loses about 60% of its incident solar radiation, the room maintains an indoor air temperature reaching 35°C, demonstrating its performance.

R. Elghamry and H. Hassan[7] conducted a research work based on a combination containing a geothermal air tube, a photovoltaic (PV) panel, a TW, a solar chimney, and a geothermal air tube to study its impact on ventilation and heating experimentally. The results suggested that this combination raised the ambient temperature to 14°C and managed to change the air in a significant way.

A. Baïri et al.[8] conducted an experimental study on a TW by incorporating vertically positioned transparent partitions. Using a scaled-down model allows us to determine the mean Nusselt Number for both cases, one without partitions and the other with partitions. The results show that these partitions are capable of enhancing convective heat transfer by up to 14%.

Ana Briga-S et al.[9] analysed the impact of ventilation openings and external shading devices, revealing from experimental data that the air layer and the massive wall exhibited a comparable oscillation pattern in temperature, surpassing 60°C. Three types of TWs in China were the subject of an experimental and numerical study of.[10] The results revealed that the type 2 wall, which is a double ventilation wall, has the highest energy efficiency. Heating efficiency for types 1, 2 and 3 was 23.8%, 32.6% and 30.5% respectively.

B. Yu et al.[11] examined a combination of thermal catalytic technology and the TW. Experimental results indicated that the air heating efficiency of the day was more than 40%. Moreover, numerical findings show that energy savings reached 97.4 kWh/m^2.

Three configurations of a modified TW, including rounded edges, sharp edges and guided airflow, were numerically analysed by[12] to predict velocity profiles, air temperatures, and heat flows through the wall for each configuration. The results revealed that energy and exercise efficiency were higher with guided airflow.

An experimental study of a TW with a storage system vertically integrated was investigated by L. Agurto et al.[13] During the cold season, its impact translates into a reduction in energy demand of almost 33%. The results revealed that the TW extends the hours of indoor thermal comfort significantly. In summer, the addition of outdoor shading elements prevents the risk of overheating, which increases the hours of comfort.

An experimental analysis of the thermal performance of a TW was carried out in Iraq by Ruqaya R et al.[14] In November, the system's highest solar fraction factor values were seen with an average factor of about 0,7, solar energy could cover about 70% of space heating needs, depending on local climatic conditions.

The thermal performance of the TW is analysed through experimental works or numerical simulations. Numerous factors can increase the thermal performance of the TW, such as the depth of the air channel, the type of glazing, the airflow velocity, insulation materials, and storage heating capacity. Using a 10 cm air gap depth increases the absorber temperature while widening the

gap decreases.[15] The glazing type and layer influence in a significant way the transfer of thermal energy in TWs. During the day, a single glass layer offers a high solar radiation gain for the wall. Compared to the double layer of glass, using a single glazing with a shutter for the nighttime will provide a more significant thermal gain to heat in the winter season.[16] The energy performance can be increased by up to 56% by introducing an insulated material to the traditional TW.[17]

The heat storage capacity of the TW can be enhanced by adding change phase materials (PCMs).[18] Shanshan Li et al.[19] conducted numerical research on the thermal performance of a TW with PCM during the winter and summer seasons. The results show that the use of a PCM TW can enhance indoor thermal comfort and decrease both cooling and heating loads throughout the whole year compared to other systems. The double layer of PCM in the TW was applied in the research work of[20] with various air gap thicknesses. They demonstrated that a 20 cm air gap can reduce energy consumption by 34%.

Enghok Leang et al.[21] investigated a numerical study of a composite TW integrating PCM. A comparison between composite TW with concrete storage wall and TW with microencapsulated wax, a PCM. The results show a significantly greater heat recovery capacity from the PCM storage wall, with an increase of over 50% compared to the concrete storage wall.

Shanshan Li et al.[22] studied numerically the thermal behaviour of a TW integrating PCM during the two-season summer and winter. The use of PCM TWs can enhance indoor thermal comfort and decrease the overall heating and cooling demand throughout the year when contrasted with classical TWs.

Zhu et al.[23] conducted a study focusing on the design of TWs with PCMs to enhance the building envelope and thermal properties throughout the year. According to the simulation results, using the TW with PCM reduced the cooling and heating loads by 9% and 15%, respectively, compared to the reference TW. In winter, the indoor temperature in the room with PCM was, on average, 0.11°C higher than the reference, while in summer, it was, on average, 3.28°C lower.

Moreover, combined PV technology and TWs have garnered more interest since they are capable of heating the spaces by collecting heat from the PV cells. After this, various theoretical and experimental investigations were conducted by J. Jie et al.[24] For instance, they conducted experimental and numerical studies to investigate the effect of different concepts for the south façade,[25] the coverage ratio of PV,[26] and airflow rate within the channel[27] on the system's performance.

Akbarzadeh et al.[28] experimentally studied a TW by varying the width of the air gap from 10 cm to 35 cm. The results showed that the width of 25 cm gave a better performance in terms of heat transfer.

Nanofluids are the most exciting topic in this day because of their enhanced thermodynamical properties, which makes them useful for enhancing heat transfer efficiency. Several investigations have been conducted about their applications and benefits.[29–33] R. Ahamed et al.[34] investigated the thermal-hydraulic performance of curved trapezoidal-corrugated channels with E-shaped baffles using single and hybrid nanofluids. The findings reveal significant enhancements in heat exchange, with increases in the Nusselt number ranging from 35% to 60% compared to water. F. Ahmad et al.[35] explored the impact of different corrugation patterns on heat transfer using single and hybrid nanofluids. The results indicate a 25%–30% increase in the heat transfer coefficient and an optimal 22.19% thermal performance. A numerical investigation was carried out to examine the flow and convective heat transfer in helically corrugated pipes using single and hybrid nanofluids by A. Mustakim et al.[36] According to simulation results, changing the shape can improve heat transfer by about 26.5%. In their investigation, Monjurul Ehsan et al.[37] looked at how Al_2O_3-water nanofluid can be utilised to increase forced convection heat transfer and minimise the pumping power in turbulent flow through rough parallel plates. The findings reveal that for rough surfaces, there are remarkable increases in heat transfer when the surface roughness and nanofluid volume fraction are increased, with an enhancement of up to 36.9%.

There have been some advances as far as the optimisation of air gap width in TW systems is concerned. However, there is evident lack of research about this topic and how it can affect thermal performance directly. Though various passive solar systems are studied and adjustments made to enhance their efficiency in the existing literature, few studies have systematically analysed effects of different widths of air on TW thermal behaviour. In most previous studies, only fixed dimensional configurations were considered without considering that variation in air gap affects the dynamics of airflow and consequently impacts heat transfer efficiency. In this work, we will numerically investigate the impact of air gap width in the TW on its thermal behaviour. We will employ numerical simulations based on computational fluid dynamics (CFD) to determine how different air gap configurations and dimensions would impact the thermal conduction through the TW. These findings will guide toward a better design and enhancement of the TW for buildings with less energy consumption. This study is quite important from an industrial aspect. Reducing traditional energy sources can be achieved by optimising the design of TW systems, which can result in significant

energy savings for building heating. This directly affects the construction sector, especially when it comes to designing energy-efficient structures.

2 | METHODS AND MATERIALS

The TW of the analysed ventilation system of the experimental setup of[38] is designed as a cubic chamber, featuring two apertures for air circulation, positioned at the upper and lower extremities. This wall is built with a concrete block 15 cm thick, forming a massive structure of height and width, having 1.6 and 2 metres, respectively. On the exterior of this wall, a ductile steel sheet with a thickness of 1 mm is fixed and painted in matte black to promote the absorption of solar heat. Inside, glass wool insulation with a thickness of 0.05 m is added to prevent overheating during hot summer periods. In addition, on the south side of the wall, a standard glass of 4 mm is installed, creating an air gap of 0.25 m, which acts as a channel for the airflow. The tangible attributes of the substances employed for TW are elaborated upon in Table 1 whilst Figure 1 represents the conventional TW design.

TABLE 1 Material properties of Trombe wall (TW).

Materials	Specific heat (J/kgK)	Thermal conductivity (W/mK)	Density (kg/m^3)
Air	1006	0.0247	1.225
Glass	800	0.8	2220
Concrete	940	1.6	1700
Glass Wool	1000	0.036	10
Steel	502.4	16.2	8030

3 | NUMERICAL MODEL

The ANSYS Fluent software is used for numerical simulations and thermal calculations.

ANSYS Fluent is a dynamic simulation software utilised for the calculation of thermal performance and energy consumption data in a building model. This software is used in this section to validate our results numerically in accordance with the experimental results of.[38]

The CFD simulation procedure for the TW model is depicted in Figure 2. Furthermore, this section provides details on the mathematical formulation, mesh generation, selection of physical models, and specification of boundary conditions employed in the TW simulations.

Steady-state modelling of heat transfer and fluid flow in a bi-dimensional setting was used under specific conditions. The flow is assumed to be incompressible, and the behaviour of density follows that of an ideal gas, with all fluid properties remaining constant.

The solar radiation was applied vertically to the glass cover. The software ANSYS FLUENT (R2.2021) was utilised for simulations, employing the Finite Volume Method (FVM) to solve the set of partial differential equations, including those governing mass conservation, energy, and momentum. The general forms of these equations are presented below.[25]

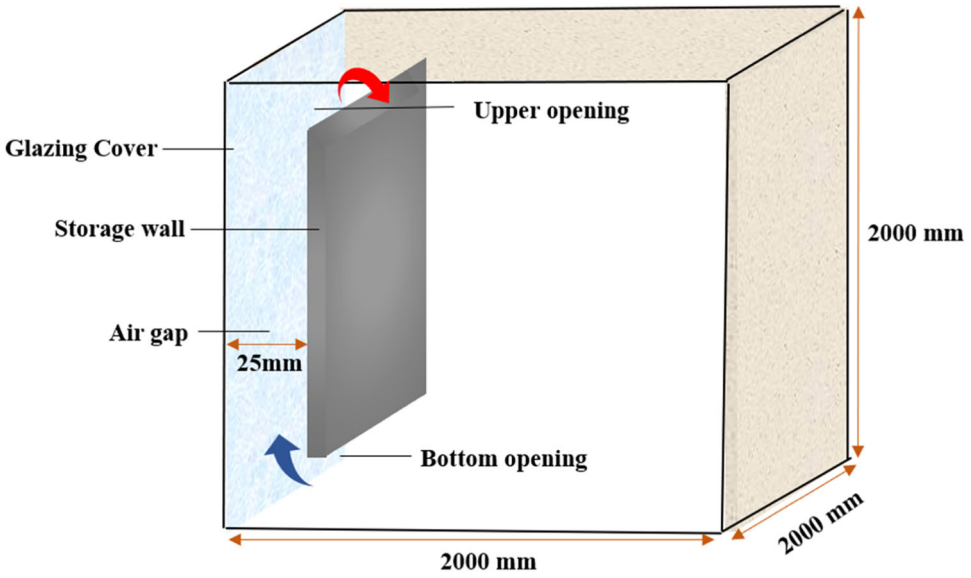

FIGURE 1 Design of standard Trombe wall.

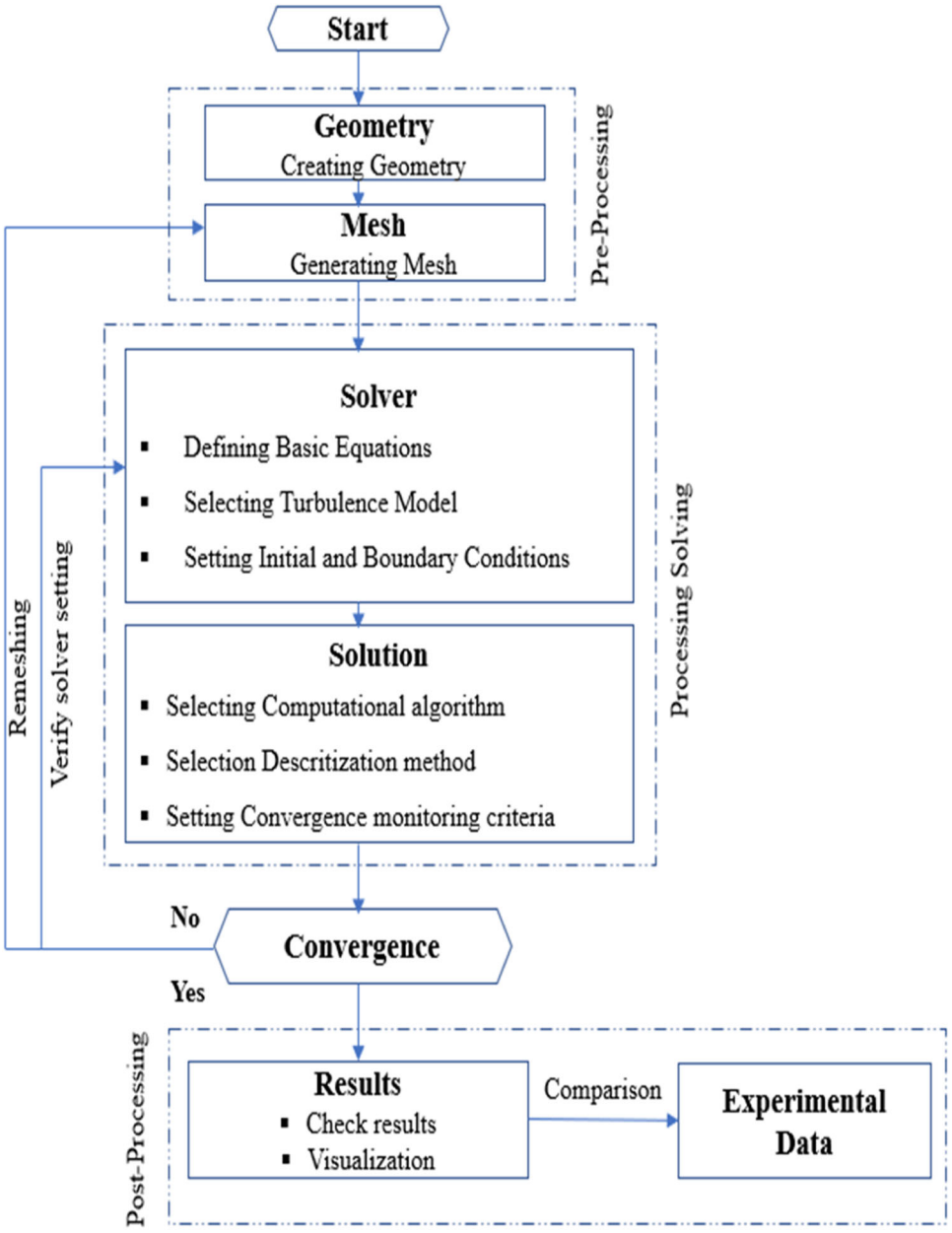

FIGURE 2 Computational fluid dynamics (CFD) process.

3.1 | Mathematical model

A 2D model has been utilised to analyse the TW, considering the following governing equations[38]:

Mass conservation is:

$$\bar{\nabla}.\,\bar{\nu} = 0 \tag{1}$$

Momentum conservation is:

$$\rho \quad \bar{\nu}\,.\nabla\bar{\nu} = \rho\bar{g} - \bar{\nabla}p + \bar{\nabla}\tau \tag{2}$$

Energy conservation is:

$$\rho \quad \mathbb{C}_f.\,\bar{\nu}\,.\,\bar{\nabla}\,T = k \quad \nabla^2 T \tag{3}$$

Where the symbol ∇ represents the partial derivative concerning spatial coordinates (x, y), ν is the velocity of the fluid, p is the static pressure, ρ means the density, g is the gravitational acceleration, τ represents the viscous stress tensor, $\mathbb{C}_f$ means specific heat capacity of the fluid at constant pressure, k is the thermal conductivity and T represents the temperature.

3.2 | Turbulence model

The formulation of the RNG k-ε turbulence model is derived from the instantaneous Navier-Stokes equation

using the mathematical method RNG. This model is more efficient for high bending flows and higher speeds compared to other models, such as the standard model based on the k-ε. The equations are given as follows[5]:

$$\frac{\partial}{\partial t}(\rho k) + \frac{\partial}{\partial x_i}(\rho k u_i) = \frac{\partial}{\partial x_j}\left[\alpha_k u_{eff}\frac{\partial k}{\partial x_j}\right] + G_k + G_b - \rho\varepsilon - Y_M + S_k \quad (4)$$

$$\frac{\partial}{\partial t}(\rho\varepsilon) + \frac{\partial}{\partial x_j}(\rho\varepsilon u_i) = \frac{\partial}{\partial x_j}\left[\alpha_\varepsilon u_{eff}\frac{\partial \varepsilon}{\partial x_j}\right] + C_{1\varepsilon}\frac{\varepsilon}{k}(G_K + C_{3\varepsilon}G_b) - C_{2\varepsilon}\rho\frac{\varepsilon^2}{k} - R_\varepsilon \quad (5)$$

When density is denoted by ρ. The turbulent kinetic energy, represented by K, and its dissipation rate ε, are both functions of time t and Cartesian coordinates (x_i) where i ranges from 1 to 3, representing the spatial directions. The velocity components in these directions are indicated by u_i. The turbulent Prandtl numbers for K and ε are represented byα_k and α_ε, respectively, and they influence the effective viscosity u_{eff} terms. G_K represents the production of turbulent kinetic energy due to mean velocity gradients and G_b for the production due to buoyancy. The dissipation of turbulent kinetic energy is captured by $\rho\varepsilon$. $Y_M$denotes the contribution of fluctuating dilatation in compressible turbulence to the overall dissipation rate.

Additional source terms for K and ε are given by S_k and R_ε, respectively. $C_{1\varepsilon}$, $C_{2\varepsilon}$ and $C_{3\varepsilon}$ are model constants in the ε equation.

3.3 | DO radiation model

From the literature, the glass is considered to be a diffuse grey medium. However, the glass cover is a semi-transparent medium. In this study, the radiation problem is solved by applying the DO model. The choice of this model was based on its performance and its capability to simulate the behaviour of light on surfaces, including absorption, emission, reflection, and transmission. This model solves the equation of radiation transport (RTE) as written below[39]:

$$\nabla.\,(I(\vec{r},\vec{s})\vec{s}) + (\alpha+\sigma_s)I(\vec{r},\vec{s}) = \frac{\sigma_s}{4\pi}\int_0^{4\pi} I(\vec{r},\vec{s}')\,\Phi(\vec{s}.\,\vec{s}')\;d\Omega' + \alpha n^2\frac{\sigma T^4}{\pi} \quad (6)$$

Where I represent the radiation intensity, α is the absorption coefficient, n is the refractive index, Φ as the phase function and Ω′ as the solid angle, $\vec{r}$ and $\vec{s}$ denote the position and direction vector, respectively. σ_s and $\vec{s}'$ are the scattering coefficient and scattering respectively. T stands for the temperature and σ represents the Stefan Boltzmann constant.

4 | MODEL AND MESH

The precision of the numeric outcomes is directly influenced by the quality of the mesh used for the simulation, especially in areas where the variables have high gradients. The 2D configuration contains 60850 nodes. To ensure a higher resolution in the areas of the system, a dense mesh was used for regions near the walls and areas with high-temperature gradients.

To obtain precise results in a CFD model that accurately reflects the geometry and experimental dimensions, a fine-structured mesh is essential, as illustrated in Figure 3. A mesh independence analysis of the calculation results was performed for a stationary configuration.

To ensure the reliability and accuracy of CFD simulations, five different cases were tested by modifying the number of elements, as shown in Figure 4, which illustrates the temperature distribution within the air gap for various mesh configurations, as determined by the maximum radiation intensity (875.3 W/m²) at noon (12 h).

This analysis allowed us to determine the optimal mesh size, which was then used consistently in all subsequent calculation steps. The two-dimensional configuration included 60,850 knots. To improve spatial resolution in critical areas of the system, a finer mesh was chosen with 0.99 of orthogonal quality. The values of each mesh are summarised in Table 2.

It appears from this Figure 4 that the temperature variation becomes almost stable from the fourth mesh. However, a slight disturbance between the cell sizes was noted; stabilisation of the results was observed for a number of elements equal to 20,000.

5 | BOUNDARIES CONDITIONS

Following the presentation of the governing equations for mass, momentum, and energy transfer, the boundary conditions specific to the TW system are established to facilitate accurate numerical simulations.

The TW is a system designed to collect heat during sunny periods. This technique causes air circulation within the airspace and enclosure, attributed to variances in density. In areas where the surfaces are hot, the airflow moves upwards because the hot air is less dense. On the other hand, when the surfaces are cold, the airflow

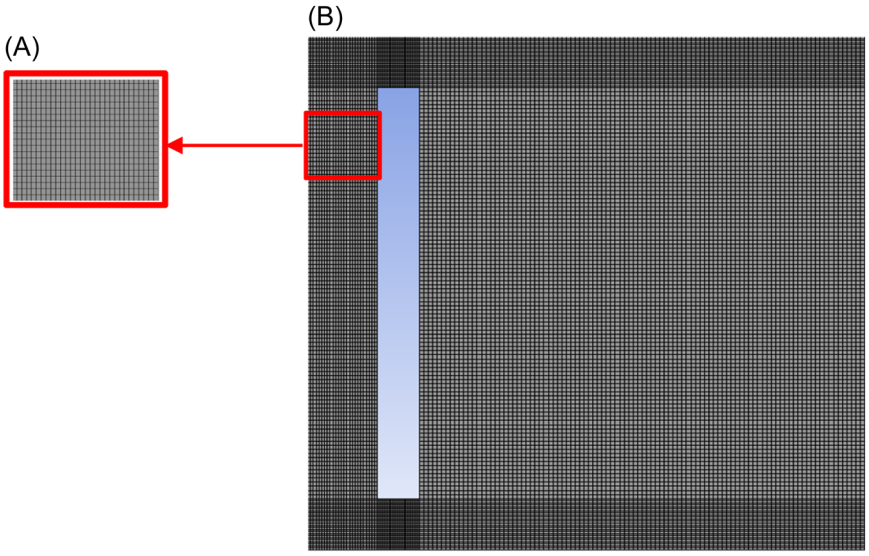

FIGURE 3 (A) Zoom meshing, (B) 2-D meshing.

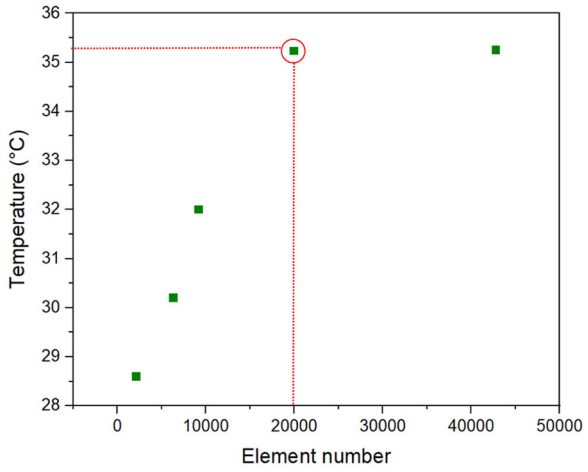

FIGURE 4 Calculated results of temperature into the room with different element number.

TABLE 2 Meshing parameters.

Mesh	Mesh1	Mesh2	Mesh3	Mesh4	Mesh5
Node number	6712	19488	28180	60850	129640
Element number	2144	6336	9200	20000	42800

changes direction and moves downwards due to the higher density of cold air.

The room was treated as an isolated space heated by direct sunlight. Glass has a convection heat transfer coefficient of 2 W/m²K and is handled as a mixed surface. The steel plate's emissivity and absorptivity are tuned to 1 and 0.9, respectively. With the exception of the glass, which is exposed to solar radiation as shown in Figure 5, solar radiation intensity, along with outdoor air temperature, is based on experimental data.[38] All walls are thought to be

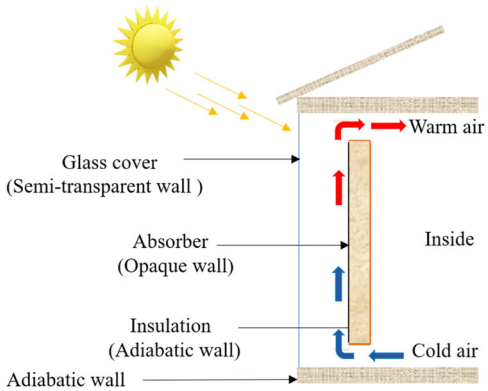

FIGURE 5 Boundary conditions of Trombe wall.

adiabatic. The following conditions are roughly aligned with the assumptions used in the numerical simulations: Since air density mostly depends on temperature and there is little variation in air pressure within the TW, the analysis makes the incompressible ideal gas assumption and assumes a stable condition. Additionally, 2-D turbulent flow is included in the simulations, and all fluid properties are maintained throughout. No thermal dissipaters exist within the heat barrier. The tangible characteristics of the material comprising the thermal partition, which are independent of temperature, are treated as constant. The heat loss from the lateral walls to the surroundings is assumed to be negligible due to its small magnitude.

6 | RESULTS AND DISCUSSIONS

6.1 | Validation model

In this setup, the system is entirely closed. This design effectively emphasises the role of natural convection as

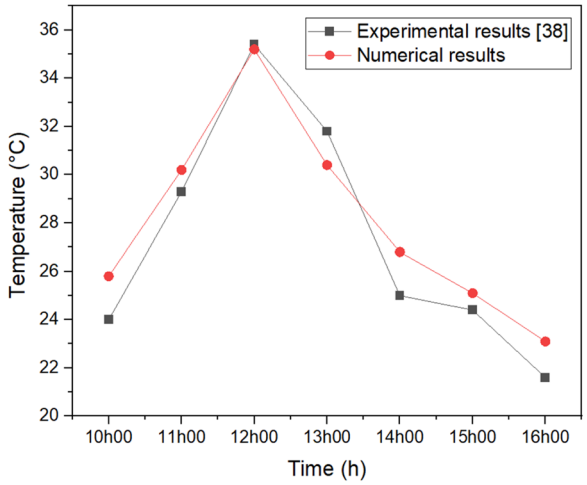

FIGURE 6 Comparison between the numerical and experimental results with regard to airflow temperature.

the primary mechanism for airflow within the room. The ambient temperature is maintained at approximately 15.5°C, creating a baseline for evaluating the thermal performance of the TW under realistic conditions. The glass wall is subjected to solar radiation of 738.31 W/m², simulating direct sunlight exposure, which is crucial for assessing the TW's ability to absorb and store heat.

Figure 6 presents the results from the numerical simulation, comparing them with the temperature data measured during the experiment.

The values demonstrate an almost constant consistency between them. By analysing the simulation against the experimental measurements. The choice of evaluation criterion was a relative error (RE). The difference between the measured values and the simulation values is calculated according to the following formula:

$$RE = \frac{Tref - Tnum}{Tref}(\%) \quad (7)$$

We can see an average RE of only 5% for the air temperature inside the air gap. This shows a particularly satisfactory correspondence between the simulated results and the actual data obtained during the experiment. Table 3 shows the relative error between the present numerical results and experimental results.[38]

An analysis of the dimensionless wall distance, Y^+ represented in Figure 7 was made and treated with care. The maximum Y^+ value calculated in our model was 0.45. This value is in an acceptable range which means the accuracy of the boundary layer thickness prediction was fine enough to capture the flow behaviour and the boundary layer during the simulation.

TABLE 3 Relative error between the numerical and experimental results.[38]

Time (h)	Experimental results[38]	Numerical results	Relative Error%
10h00	24	25.8	7.5
11h00	29.3	30.2	3.0
12h00	35.4	35.2	0.5
13h00	31.8	30.4	4.4
14h00	25	26.8	7.2
15h00	24.4	25.1	2.8
16h00	21.6	23.1	6.9

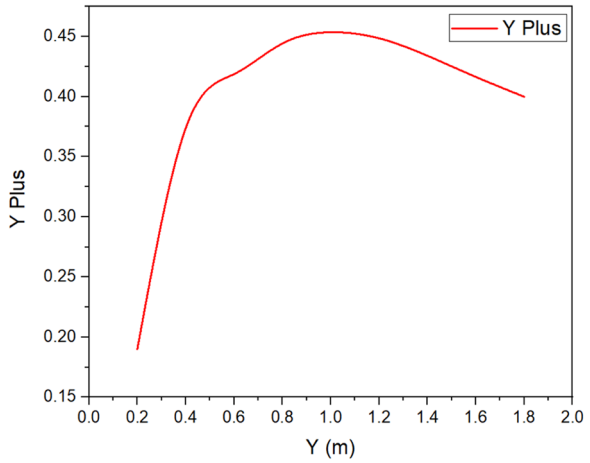

FIGURE 7 Y Plus evolution over the absorber.

7 | INFLUENCE OF AIRSPACE BREADTH ON TEMPERATURE AND SPEED BEHAVIOUR

In the present study, a variable evaluation is performed to predict the effect of airspace thickness from 0.05 m to 0.3 m on the thermal performance of a TW simulated with 15.5°C of ambient temperature and 738.31 W/m² as boundary conditions. The numerical results obtained from the CFD model are used to closely examine the influence of the air gap. The change was made in terms of geometry, as shown in Figure 8, designed by the software DESIGN MODELER, and all operational parameters remained constant. This change has led to improvements in the thermal performance of the system. In equilibrium, a comparison of the thermal performances of the different air widths of the system in heating mode was performed.

A comparison of the thermal performances of different air gap widths in heating applications was conducted.

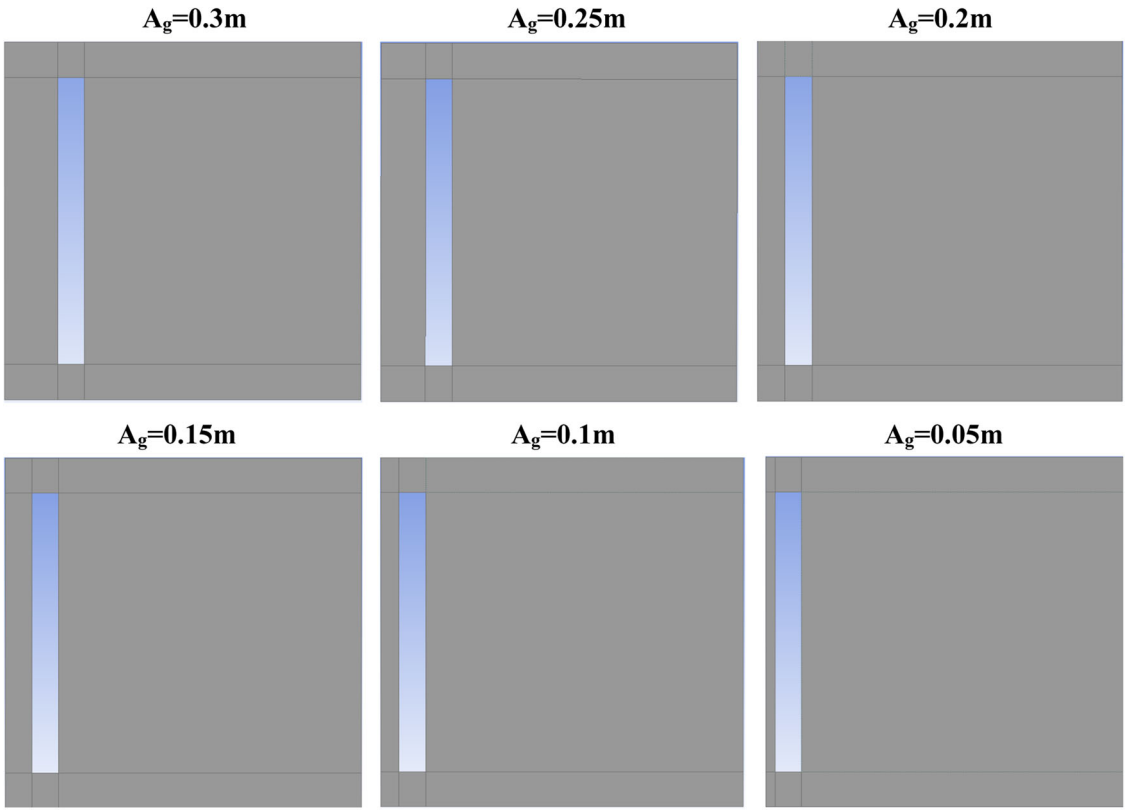

FIGURE 8 Trombe wall configurations with different air gap widths.

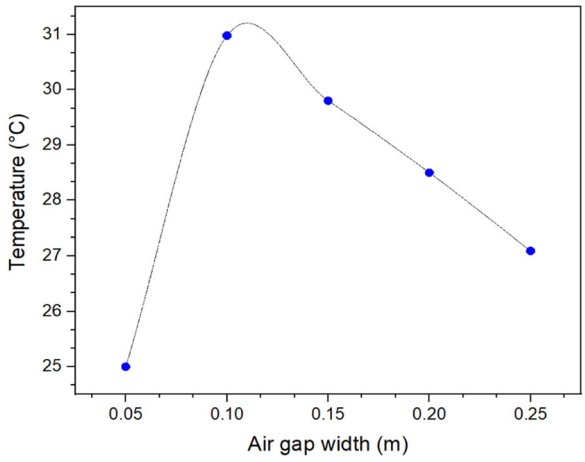

FIGURE 9 Temperature distribution for different air gap widths at 738.31 W/m².

7.1 | Temperature distribution

Figure 9 illustrates the temperature distribution across the six air gaps of the studied TW. The thermal level of the storage wall can be consistently higher at various locations, repeating consistently across all observed deviations. This can be attributed to the absorbing layer of the massive wall, which receives higher radiation intensity.

An evident observation is the substantial difference in air temperatures between the upper and lower parts of the chamber. Given that the entrance can be positioned close to the lower wall section, that discrepancy is expected. As air ascends within the cavity, it progressively absorbs more heat.

The temperature inside the cavity and at the absorber reaches its maximum value when The breadth of the airspace is 0.1 m to exceed 30°C at 10:00 h. As the space between the glass cover and the absorbent plate decreases, the temperature also increases. This temperature difference can be attributed to the increase in mass flow of air as the air gap widens, leading to the cooling of the absorber and improved ventilation of the room. In theory, widening the air gap should increase air flow, thereby facilitating more excellent absorption of heat in the form of solar energy.

There is very little space in which the air can move, so it reduces heat transfer between the air around the absorbing material, leading to overheating of the absorbing body when the gap between them is 0.05 m wide. Eventually, this makes solar heating systems less efficient than they should be.

The temperature contours are shown in Figure 10, reflecting the same distribution as the absorber in Figure 11, representing the temperature throughout the length of the absorber (Y). It is evident that the

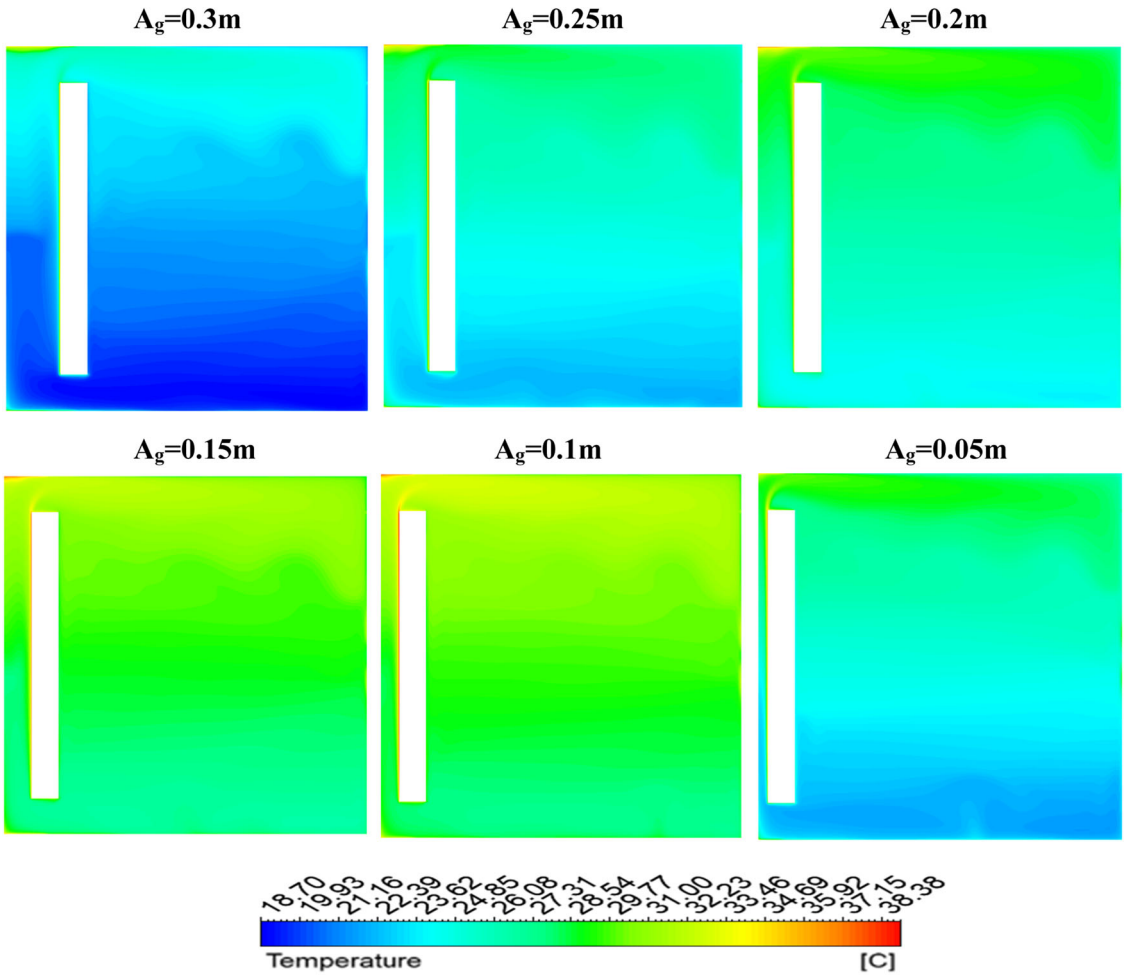

FIGURE 10 Temperature contours for different air gap widths.

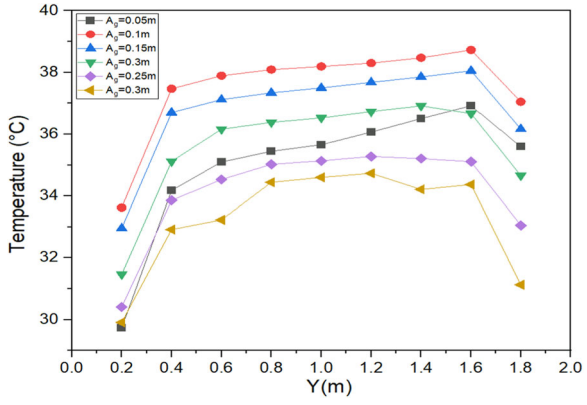

FIGURE 11 Absorber temperature for different air gap widths.

temperature is lower for lower regions and higher for higher areas. It reaches its maximum when the air gap is set at 0.1 m to achieve 30°C in the air gap while it does not exceed 23.9 compared to experimental results.

The Y-direction exhibits the largest temperature gradient compared to other directions.

7.2 | Velocity distribution

The velocity field for each airflow width is illustrated in Figure 12. Notably, the speed increases within the flow passage. This increase is due to the reduction in the cross-sectional area as air moves through the wall's channel, which accelerates the flow. The flattening of the velocity profile along the entrance section of the wall is due to turbulence in the flow. Turbulent flows tend to mix more, producing a more even velocity distribution throughout the flow, due to chaotic air movement. At the entrance and inside the chamber, air velocity is less than at its exit. The main reason for this is buoyancy which creates an upward moving air mass. Warmer air becomes less dense; thus, it rises making its upper part move faster compared to its lower regions.

The maximum speed recorded does not exceed 0.26 m/s due to the limitations of natural convection. Even at this relatively low velocity, effective heat transfer can still occur, aiding in the overall thermal performance of the TW.

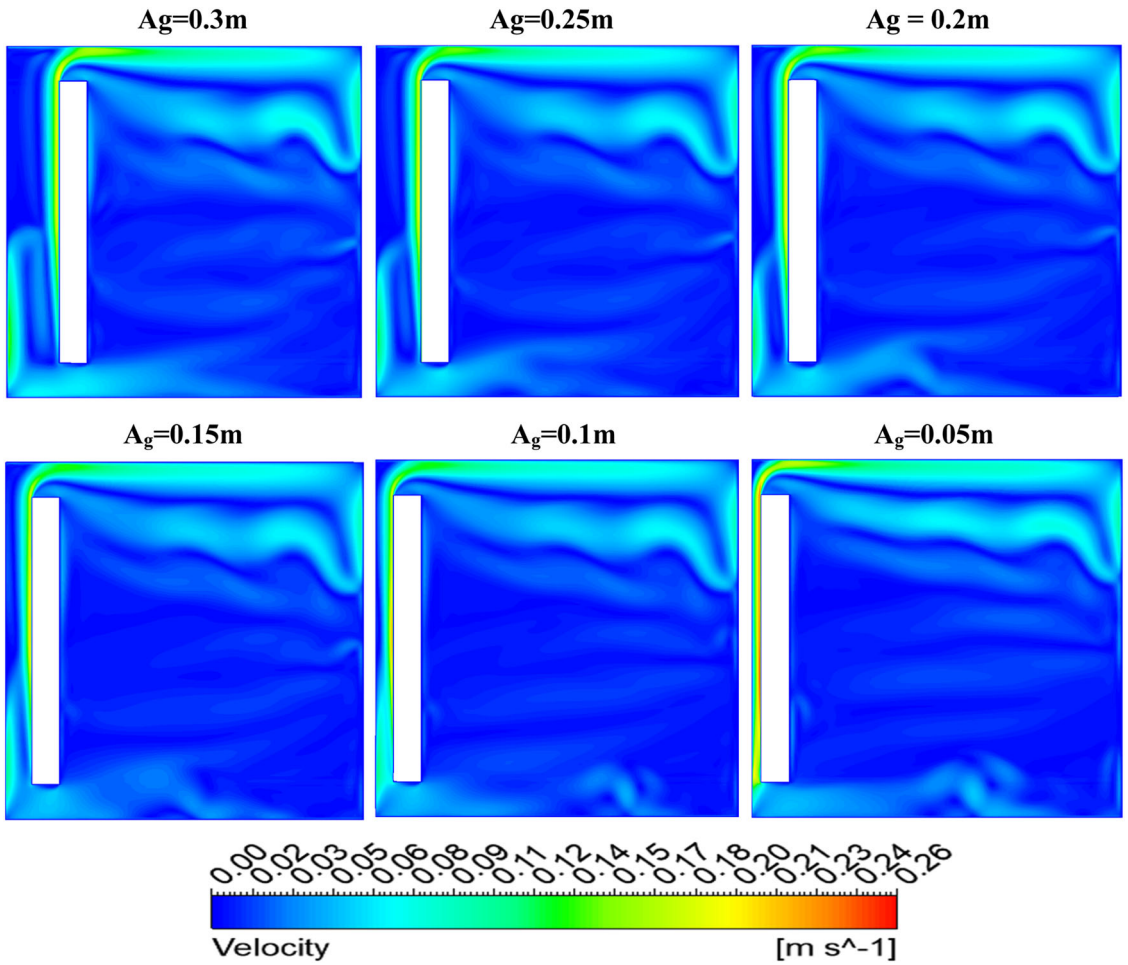

FIGURE 12 Velocity contours for different air gap widths.

7.3 | Pressure distribution

It is predominantly hydrostatic pressure distribution shown in Figure 13, though slightly lower than atmospheric pressure, especially seen at the bottom of the TW, a circumstance which can be attributed to the losses occurring at the entrance restriction. At locations where the inlet and outlet pressure of TW is low, there is a clear difference in pressure distribution between the air gap and the room.

8 | THERMAL EFFICIENCY

The performance of a TW can be measured using thermal efficiency.

Efficiency is determined by assessing the amount of heat energy gained by the air in the air cavity, relative to the total solar radiation received. Instantaneous thermal efficiency can be defined as follows[11]:

$$\eta = \frac{\dot{m}\, C_p\, (T_{out} - T_{in})}{A\, I} \tag{8}$$

Where $\dot{m}$ refers to the mass flow rate of air in the air cavity, and C_p denotes the specific heat capacity of air. T_{out}, T_{in} represent the outlet and inlet air temperatures, respectively. The area receiving solar energy is denoted by A and I is the intensity of solar radiation.

Figure 14 illustrates how thermal efficiency varies across different configurations under the same conditions over a single radiation intensity of 738 W/m^2. It is observed that the thermal efficiency of all configurations improves as the air gap width decreases from 0.3 m to 0.1 m.

It is noticed that the thermal efficiency for the configurations with 0.2 m, 0.15 m, 0.1 m, and 0.05 m air gap width is higher than the geometry of Abdeen et al.,[38] and the highest thermal efficiency exceeded 37%. Once air is kept in an area that is too small, its convection takes place faster, making it more effective in transferring heat between areas.

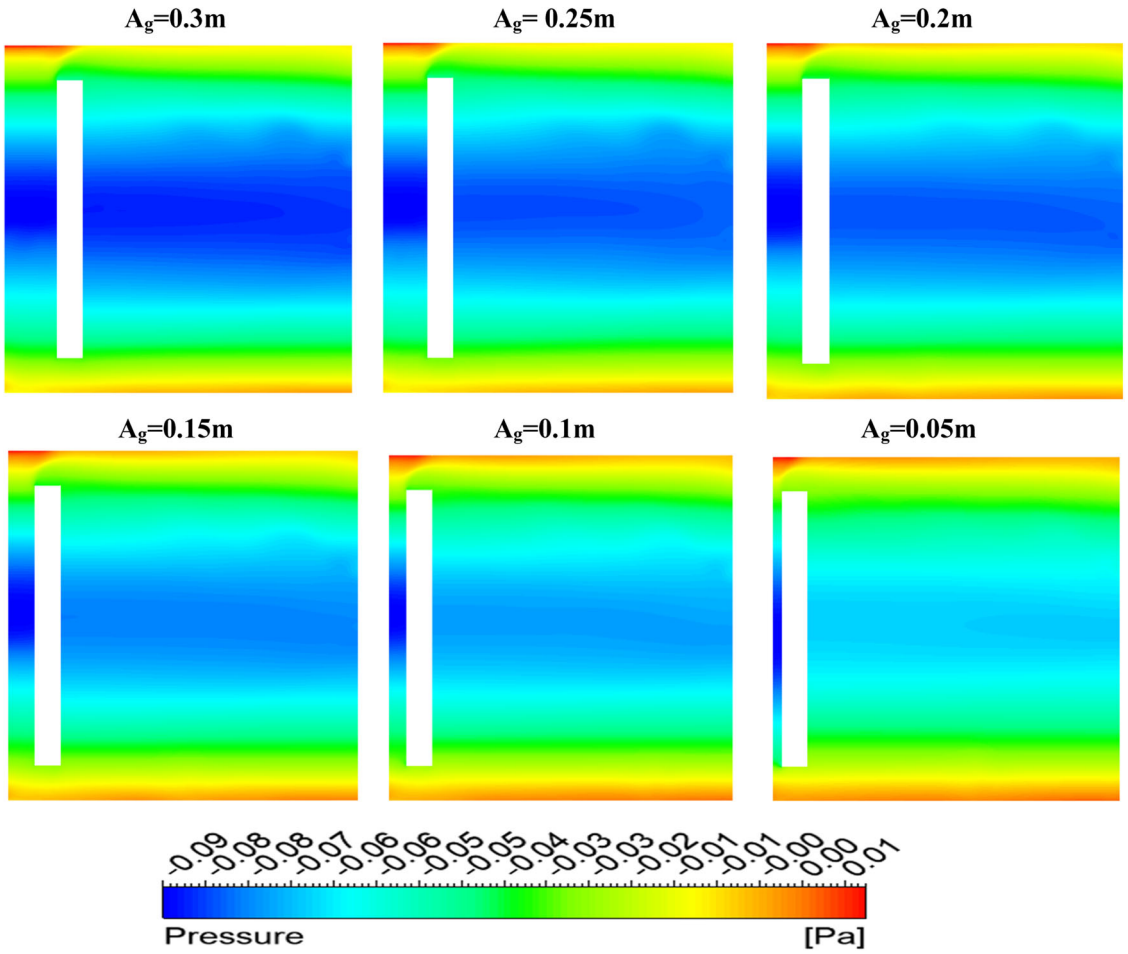

FIGURE 13 Pressure distribution for different air gap.

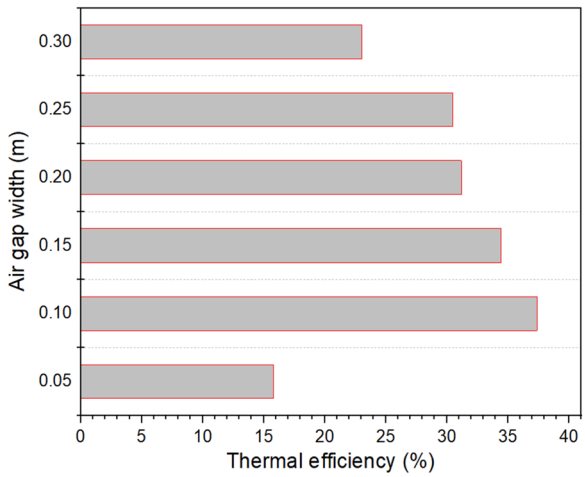

FIGURE 14 Thermal efficiency of different air gaps.

The air gap's effect on efficiency is quite significant: as the air gap increases, efficiency tends to decrease.

Further insights into the thermal efficiency of TWs are provided in Table 4, which offers an overview of various studies of the TW system.

TABLE 4 Overview of some studies of Trombe wall's thermal efficiency.

Authors	Thermal efficiency
M. Rabani et al.[40]	25%
Koyunbaba et al.[41]	4.52%–27.2%
J. Jie et al.[17]	33.85%
Dimassi and Dehmani[42]	31.7%
A.A. Hassanain et al.[43]	27.1%
This study	15.82%–37.45%

9 | CONCLUSION

This study aims to investigate the TW system within different air gap widths while validating the simulation model against experimental results from.[38] Comparisons of experimental and simulated findings show good agreement, with errors of no more than 6.5%. Thus, the simulation model is considered valid under the specified boundary

parameters. The system CFD modelling is derived from empirical data acquired in Egypt in 2019, with a focus on steady-state analysis. As a result, the numerical model serves as a viable alternative to experimentation, drastically lowering the need for additional experimental trials and facilitating progress in TW research.

The configuration featuring a 0.1 m of air gap width has been chosen as the optimal option, the temperature exceeds 30°C in the air gap at 10:00 AM with 738.31 W/m².

10 | FUTURE SCOPE

There is a great need for future research about TW systems to tackle the dynamic environmental conditions, investigate new materials such as PCMs and nanofluids, and evaluate the long-term performance and durability of these systems. Moreover, it will be necessary to enlarge the TW optimised system depending on various types of buildings; carry out deep analysis regarding energy efficiency and cost-effectiveness; plus include a smart control system to enhance energy utilisation. In this way, it will be possible to completely develop the potentiality of TW systems that will result in more climate-adaptable and eco-friendly buildings across various climates. The utilisation of extended surfaces (fins) in TW systems is of vital importance to enhance the heat transfer between the absorber surface and the heat transfer fluid. This is not limited to TW systems as can be seen a wide range of applications in other renewable energy technologies like solar thermal applications.[44] It is already proved that the fins improve the thermal performance figures of such applications.[45] In this regard, it is important to note that optimised fin designs and operational conditions[46–48] need to be taken into consideration for optimum performance enhancement from TW systems. The next works can focus on such aspects for further performance enhancement of TW technologies.

NOMENCLATURE

A	Area [m²]
α	Absorption coefficient
α_k	Effective Prandtl value of K
α_ε	Effective Prandtl value of ε
C_f	Specific heat capacity of the fluid [kJ/kgK]
C_p	Specific heat capacity [J/(kgK)]
$C_{1\varepsilon}$	Model constant for ε
$C_{2\varepsilon}$	Model constant for ε
$C_{3\varepsilon}$	Model constant for ε
$\dot{m}$	Mass flow rate [kg/s]
ε	Rate of turbulent kinetic energy dissipation [m²/s³]
g	Gravitational acceleration [m/s²]
G_b	Production of K due to buoyancy
G_k	Source of turbulent kinetic energy attributed to the mean velocity gradient
I	radiation intensity [W/m²]
K	Turbulent kinetic energy [J/kg]
k	Thermal conductivity [W/mK]
n	Refractive index
Ω'	Solid angle
p	Static pressure [Pa]
Φ	Phase function
ρ	Fluid density [kg/m³]
σ	Stefan Boltzmann constant
σ_s, $\vec{s}'$	Scattering coefficients
S_k	Source term
T	Temperature [K]
T_{in}	Inlet temperature [K]
$Tnum$	Numerical Temperature [K]
T_{out}	Outlet temperature [K]
$Tref$	Reference Temperature [K]
τ	Viscous stress tensor
$\vec{r}$	Position vector
$\vec{s}$	Direction vector
v	Fluid Velocity [m/s]
x, y, z	Spatial coordinates
Y_M	Contribution of fluctuating dilatation in compressible turbulence to the overall dissipation rate

ACKNOWLEDGEMENTS

The authors extend their appreciation to the Deanship of Research and Graduate Studies at King Khalid University for funding this work.

ORCID

Erdem Cuce http://orcid.org/0000-0003-0150-4705

REFERENCES

1. Luo Y, Zhang L, Liu Z, Yu J, Xu X, Su X. Towards net zero energy building: the application potential and adaptability of photovoltaic-thermoelectric-battery wall system. *Appl Energy*. 2020;258:114066. doi:10.1016/j.apenergy.2019.114066
2. Bellos E, Tzivanidis C, Zisopoulou E, Mitsopoulos G, Antonopoulos KA. An innovative Trombe wall as a passive heating system for a building in Athens—a comparison with the conventional Trombe wall and the insulated wall. *Energy Build*. 2016;133:754-769. doi:10.1016/j.enbuild.2016.10.035
3. Abbassi F, Dimassi N, Dehmani L. Energetic study of a Trombe wall system under different Tunisian building configurations. *Energy Build*. 2014;80:302-308. doi:10.1016/j.enbuild.2014.05.036
4. Hu Z, Zhang S, Hou J, et al. An experimental and numerical analysis of a novel water blind-Trombe wall system. *Energy Convers Manage*. 2020;205:112380. doi:10.1016/j.enconman.2019.112380

5. Du L, Ping L, Yongming C. Study and analysis of air flow characteristics in Trombe wall. *Renewable Energy*. 2020;162:234-241. doi:10.1016/j.renene.2020.08.040
6. Hernández-López I, Xamán J, Chávez Y, Hernández-Pérez I, Alvarado-Juárez R. Thermal energy storage and losses in a room-Trombe wall system located in Mexico. *Energy*. 2016;109:512-524. doi:10.1016/j.energy.2016.04.122
7. Sci-Hub. Experimental investigation of building heating and ventilation by using Trombe wall coupled with renewable energy system under semi-arid climate conditions. *Sol Energy*. 2020;201:63-74. doi:10.1016/j.solener.2020.02.087
8. Baïri A, Martín-Garín A, Adeyeye K, She K, Millán-García JA. Enhancement of natural convection for improvement of Trombe wall performance. An experimental study. *Energy Build*. 2020;211:109788. doi:10.1016/j.enbuild.2020.109788
9. Briga Sá A, Boaventura-Cunha J, Lanzinha J-C, Paiva A. An experimental analysis of the Trombe wall temperature fluctuations for high range climate conditions: influence of ventilation openings and shading devices. *Energy Build*. 2017;138:546-558. doi:10.1016/j.enbuild.2016.12.085
10. Ma Q, Wang X, Chen X, Fukuda H, Gao W, Wei X. An experimental and numerical analysis of the thermal performance of double-layer Trombe walls. *Energy sources, part A: recovery, utilization, and environmental effects*, 2021:1-16. doi:10.1080/15567036.2021.1939463
11. Yu B, He W, Li N, et al. Experimental and numerical performance analysis of a TC-Trombe wall. *Appl Energy*. 2017;206:70-82. doi:10.1016/j.apenergy.2017.08.171
12. Corasaniti S, Manni L, Russo F, Gori F. Numerical simulation of modified Trombe-Michel walls with exergy and energy analysis. *Int Commun Heat Mass Transfer*. 2017;88:269-276. doi:10.1016/j.icheatmasstransfer.2017.09.005
13. Agurto L, Allacker K, Fissore A, Agurto C, De Troyer F. Design and experimental study of a low-cost prefab Trombe wall to improve indoor temperatures in social housing in the Biobío region in Chile. *Sol Energy*. 2020;198:704-721. doi:10.1016/j.solener.2020.02.003
14. Rustum RR, Al-Nadawi AD. Using the utility method—F-scheme in studying the long-term thermal performance of the heat-storage and transmitting wall (Trombe wall). *Wasit J Engineer Sci*. 2022;10:69-82. doi:10.31185/ejuow.Vol10.Iss2.261
15. Abbas EF, Al-abady A, Raja V, AL-bonsrulah HAZ, Al-Bahrani M. Effect of air gap depth on Trombe wall system using computational fluid dynamics. *Int J Low-Carbon Technol*. 2022;17:941-949. doi:10.1093/ijlct/ctac063
16. Kundakci Koyunbaba B, Yilmaz Z. The comparison of Trombe wall systems with single glass, double glass and PV panels. *Renew Energy*. 2012;45:111-118. doi:10.1016/j.renene.2012.02.026
17. Ji J, Luo C, Sun W, Yu H, He W, Pei G. An improved approach for the application of Trombe wall system to building construction with selective thermo-insulation façades. *Sci Bulletin*. 2009;54(no. 11):1949-1956. doi:10.1007/s11434-009-0353-6
18. Duan S, Wang L, Zhao Z, Zhang C. Experimental study on thermal performance of an integrated PCM Trombe wall. *Renew Energy*. 2021;163:1932-1941. doi:10.1016/j.renene.2020.10.081
19. Li S, Zhu N, Hu P, Lei F, Deng R. Numerical study on thermal performance of PCM Trombe wall. *Energy Procedia*. 2019;158:2441-2447. doi:10.1016/j.egypro.2019.01.317
20. Askari M, Jahangir MH. Evaluation of thermal performance and energy efficiency of a Trombe wall improved with dual phase change materials. *Energy*. 2023;284:128587. doi:10.1016/j.energy.2023.128587
21. Leang E, Tittelein P, Zalewski L, Lassue S. Numerical study of a composite Trombe solar wall integrating microencapsulated PCM. *Energy Procedia*. 2017;122:1009-1014. doi:10.1016/j.egypro.2017.07.467
22. Li S, Zhu N, Hu P, Lei F, Deng R. Numerical study on thermal performance of PCM Trombe wall. *Energy Procedia*. 2019;158:2441-2447. doi:10.1016/j.egypro.2019.01.317
23. Zhu N, Li S, Hu P, Lei F, Deng R. Numerical investigations on performance of phase change material Trombe wall in building. *Energy*. 2019;187:116057. doi:10.1016/j.energy.2019.116057
24. Jie J, Hua Y, Wei H, Gang P, Jianping L, Bin J. Modeling of a novel Trombe wall with PV cells. *Build Environ*. 2007;42(no. 3):1544-1552. doi:10.1016/j.buildenv.2006.01.005
25. Sun W, Ji J, Luo C, He W. Performance of PV-Trombe wall in winter correlated with south façade design. *Appl Energy*. 2011;88(no. 1):224-231. doi:10.1016/j.apenergy.2010.06.002
26. Jiang B, Ji J, Yi H. The influence of PV coverage ratio on thermal and electrical performance of photovoltaic-Trombe wall. *Renew Energy*. 2008;33(no. 11):2491-2498. doi:10.1016/j.renene.2008.02.001
27. Jie J, Hua Y, Gang P, Bin J, Wei H. Study of PV-Trombe wall assisted with DC fan. *Build Environ*. 2007;42(no. 10):3529-3539. doi:10.1016/j.buildenv.2006.10.038
28. Akbarzadeh A, Charters WWS, Lesslie DA. Thermocirculation characteristics of a Trombe wall passive test cell. *Sol Energy*. 1982;28(no. 6):461-468. doi:10.1016/0038-092X(82)90317-6
29. Salehin S, Monjurul Ehsan M, Rafat Faysal S, Sadrul Islam AKM. Utilization of nanofluid in various clean energy and energy efficiency applications. In: Khan MMK, Chowdhury AA, Hassan NMS, eds. *In green energy and technology. Application of thermo-fluid processes in energy systems*. Springer Singapore; 2018:3-33. doi:10.1007/978-981-10-0697-5_1
30. Monjurul Ehsan M, Noor S, Salehin S, Sadrul Islam AKM. Application of nanofluid in heat exchangers for energy savings. *Thermofluid modeling for energy efficiency applications*. Elsevier; 2016:73-101. doi:10.1016/B978-0-12-802397-6.00004-X
31. Ahmad F, Mahmud S, Ehsan MM, Salehin M. Thermo-hydrodynamic performance evaluation of double-dimpled corrugated tube using single and hybrid nanofluids. *Int J Thermofluids*. 2023;17:100283. doi:10.1016/j.ijft.2023.100283
32. Awais M, Saad M, Ayaz H, Ehsan MM, Bhuiyan AA. Computational assessment of nano-particulate (Al2O3/Water) utilization for enhancement of heat transfer with varying straight section lengths in a serpentine tube heat exchanger. *Therm Sci Engineer Progress*. 2020;20:100521. doi:10.1016/j.tsep.2020.100521
33. Islam SMNU, Mustakim A, Ahamed R, Salehin M, Ehsan MM. Advanced thermo-hydraulic assessment of helical pipes with different shapes of jackets using single-phase and hybrid nanofluids. *Int J Thermofluids*. 2024;22:100628. doi:10.1016/j.ijft.2024.100628
34. Ahamed R, Salehin M, Ehsan MM. Thermal-hydraulic performance and flow phenomenon evaluation of a curved trapezoidal corrugated channel with E-shaped baffles implementing hybrid nanofluid. *Heliyon*. 2024;10(no. 7):e28698. doi:10.1016/j.heliyon.2024.e28698
35. Ahmad F, Mahmud S, Ehsan MM, Salehin M. Numerical assessment of nanofluids in corrugated minichannels: flow phenomenon and advanced thermo-hydrodynamic

analysis. *Int J Thermofluids*. 2023;20:100449. doi:10.1016/j.ijft.2023.100449
36. Mustakim A, Islam SMNU, Ahamed R, Salehin M, Ehsan MM. Numerical assessment of advanced thermo-hydrodynamic characteristics of nanofluid inside a helically featured straight pipe. *Int J Thermofluids*. 2024;21:100591. doi:10.1016/j.ijft.2024.100591
37. Ehsan MM, Salehin M, Islam AKMS. Investigation of thermal and hydrodynamic behaviour of Al2O3-water nanofluid through a rough parallel plate. *Int J Automotive Mech Engineer*. 2017;14(3):4432-4447. doi:10.15282/ijame.14.3.2017.4.0351
38. Abdeen A, Serageldin AA, Ibrahim MGE, El-Zafarany A, Ookawara S, Murata R. Experimental, analytical, and numerical investigation into the feasibility of integrating a passive Trombe wall into a single room. *Appl Therm Eng*. 2019;154:751-768. doi:10.1016/j.applthermaleng.2019.03.090
39. Zhou L, Wang Y, Huang Q. Parametric analysis on the performance of flat plate collector with transparent insulation material. *Energy*. 2019;174:534-542. doi:10.1016/j.energy.2019.02.168
40. Rabani M, Rabani M, Rabani R, Kalantar V. Cooling performance of a new designed Trombe wall integrated with solar chimney, water spraying system, and rectangular thermal fin arrays: an experimental approach. *Int J Design Nature Ecodynam*. 2020;15(3):373-391. doi:10.18280/ijdne.150311
41. Koyunbaba BK, Yilmaz Z, Ulgen K. An approach for energy modeling of a building integrated photovoltaic (BIPV) Trombe wall system. *Energy Build*. 2013;67:680-688. doi:10.1016/j.enbuild.2011.06.031
42. Dimassi N, Dehmani L. Thermal efficiency of a solar wall in Tunisia. *Int Sch Res Notices*. 2012;2012:e465249. doi:10.5402/2012/465249
43. Hassanain AA, Hokam EM, Mallick TK. Effect of solar storage wall on the passive solar heating constructions. *Energy Build*. 2011;43(no. 2-3):737-747. doi:10.1016/j.enbuild.2010.11.020
44. Cuce E, Cuce PM. Theoretical investigation of hot box solar cookers having conventional and finned absorber plates. *Int J Low-Carbon Technol*. 2015;10(3):238-245.
45. Cuce E. Improving thermal power of a cylindrical solar cooker via novel micro/nano porous absorbers: a thermodynamic analysis with experimental validation. *Sol Energy*. 2018;176:211-219.
46. Cuce E, Cuce PM. Homotopy perturbation method for temperature distribution, fin efficiency and fin effectiveness of convective straight fins with temperature-dependent thermal conductivity. Proc Instit Mech Engineer C: J Mechan Engineer Sci. 2013;227(8):1754-1760.
47. Mert Cuce P, Cuce E. Optimization of configurations to enhance heat transfer from a longitudinal fin exposed to natural convection and radiation. *Int J Low-Carbon Technol*. 2014;9(4):305-310.
48. Panchal H, Sohani A, Van Nguyen N, et al. Performance evaluation of using evacuated tubes solar collector, perforated fins, and pebbles in a solar still – experimental study and CO2 mitigation analysis. *Environ Sci Pollut Res*. 2023;30(5):11769-11784.

How to cite this article: Friji K, Ghriss O, Bouabidi A, Cuce E, Alshahrani S. CFD analysis of the impact of air gap width on Trombe wall performance. *Energy Sci Eng*. 2024;12:4598-4612. doi:10.1002/ese3.1913